
Tourmaline records the hydrothermal events related to Zn-Pb mineralization around the Murguía diapir (Basque Cantabrian Basin, N Spain)

R. Galdos¹ A. Canals^{2*} E. Cardellach³ J. Perona⁴

¹**Faculty of Sciences and Engineering, Pontificia Universidad Católica del Perú**
Av. Universitaria 1801, San Miguel, Lima 15088, Perú. E-mail: rgaldosp@pucp.edu.pe

²**Departament de Mineralogia, Petrologia i Geologia Aplicada, Universitat de Barcelona**
C/ Martí i Franquès, s/n, 08028 Barcelona, Spain. E-mail: angelscanals@ub.edu

³**Departament de Geologia, Universitat Autònoma de Barcelona**
Edifici Cs, 08193 Cerdanyola del Vallès, Spain. E-mail: esteve.cardellach@uab.cat

⁴**Centres Científics i Tecnològics, Universitat de Barcelona**
C/ Lluís Solé i Sabarís, 1-3, 08028 Barcelona, Spain. E-mail: jperona@ub.edu

*Corresponding author

| A B S T R A C T |

The chemical composition of tourmaline has been used as a host environment register as well as a potential exploration tool for mineral deposits. In this study, the textural and chemical composition of tourmalines associated with Zn-Pb mineralizations around the Murguía diapir (Basque Cantabrian Basin, N Spain) are examined to verify if they record the mineralizing events in the area. Petrographically, tourmalines have been differentiated between inherited and authigenic. Colorless authigenic tourmalines are present as halos partially around green and pleochroic detrital grains or as individual crystals. Inherited and authigenic tourmalines are also chemically distinct. Authigenic tourmalines show different X-site occupancies, a Mg/(Mg+Fe) ratio above 0.77, and are aluminum rich and plot to the right of the povondraite-oxidravite join, above the schorl-dravite join. Inherited tourmalines plot within the alkaline (Na+K) group field, and have a Mg/(Mg+Fe) ratio below 0.77. These data suggest that authigenic tourmalines grew under reducing conditions, compatible with the hydrothermal event responsible for the ore deposition and caprock formation during the diapir ascent.

KEYWORDS | Tourmaline. Salt diapir. Zn-Pb deposits. Basque Cantabrian Basin.

INTRODUCTION

In the Basque Cantabrian Basin (BCB), Zn-Pb mineralizations associated with salt diapirs of Triassic age are found. They are interesting not only from an economic point of view, but also for their possible relationship with Mississippi Valley Type deposits that are of economic relevance in the BCB (*e.g.* Reocín, Txomin). According to Perona *et al.* (2018), these mineralizations are of peridiapiric type, located in the Carbonate Transition Zone (CTZ) and in the detrital materials of the Valmaseda Formation (Fm.) (Lower Cretaceous). Tourmaline has been recognized as an accessory mineral in both lithologies (Perona *et al.*, 2018).

Tourmaline is a chemically and mechanically stable mineral that forms over a wide range of pressure and temperature conditions and its crystalline structure allows it to incorporate a large number of mono-, di-, tri-, and tetravalent cations, as well as mono- and divalent anions (Dutrow and Henry, 2011; von Goerne *et al.*, 2001). It often presents chemical zoning and/or overgrowths and, since it shows negligible intercrystalline diffusion of major and trace elements, it can record information about the different mineral growth environments (Griffin *et al.*, 1996; Slack and Trumbull, 2011; van Hinsberg *et al.*, 2011).

The present work focuses on the study of tourmalines that occur in association with Zn-Pb-(Ba) occurrences at Altube, Jugo, and Iturlum, located around the Murguía diapir (Fig. 1). The aim of this paper is to assess the potential of tourmaline optical and chemical zoning as a tool to trace mineralizing fluids in hydrothermal environments associated with sedimentary basins.

GEOLOGICAL SETTING

The BCB is related to rift systems that developed between the European and Iberian plates during Mesozoic times (Tavani and Muñoz, 2012; and references therein). The Mesozoic stratigraphic record includes sedimentary rocks from the Triassic to the Upper Cretaceous. The fault activity during the rifting event that began in the Late Jurassic led to the deposition of a thick succession of sedimentary rocks, mainly during the Early Cretaceous. The Aptian-Albian period was characterized by the deposition of a thick sequence of shallow-platform limestones and siliciclastics (*e.g.* microconglomerates, sandstones, and calcarenites of the Valmaseda Fm.). These sequences are intruded by diapirs of evaporitic rocks of

Upper Triassic age, aligned along NW-SE and NE-SW structures (Fig. 1A). Among these, the Murguía diapir is an outstanding example, whose ascent initiated during Early Cretaceous times and continued up to Santonian times.

Vein and stratabound Zn-Pb-(Ba) occurrences are hosted within the Valmaseda Fm. and the CTZ at the margins of the Murguía diapir (Altube, Jugo, and Iturlum; Fig. 1B). The CTZ corresponds to a cackrock modified by dolomitizing and mineralizing hydrothermal fluids. Mineralization consists of disseminated-to-massive sulfides, which replace the carbonate matrix and lithoclasts of the Valmaseda Fm., and the carbonates of the CTZ. Paragenetically, barite predates sulfides (sphalerite, galena, pyrite/marcasite), which are contemporaneous with dolomitization. Tourmaline appears as an accessory phase in both the detrital rocks of the Valmaseda Fm. and in the carbonates of the CTZ (Perona *et al.*, 2018).

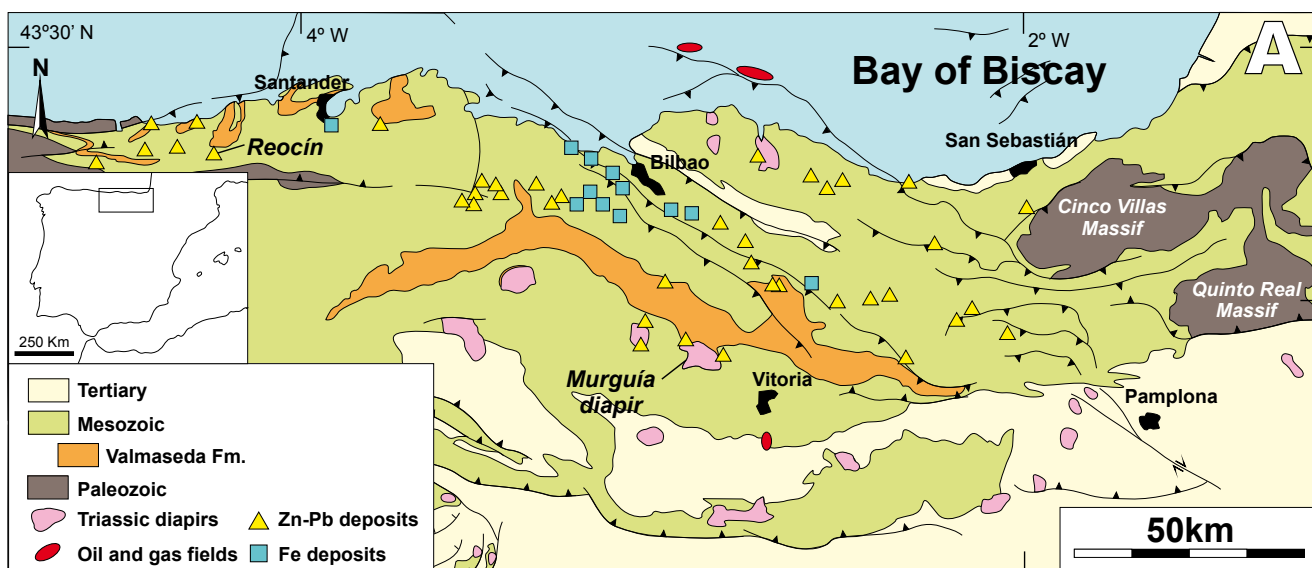
SAMPLING AND METHODS

Thirty-three thin sections were selected for this study: 15 from the Altube area (8 from the CTZ and 7 from the Valmaseda Fm. 11 from the CTZ at Jugo, and 7 from the CTZ at Iturlum. Samples came from drill cores of an exploration drilling program conducted in 1997 and 1998 at Altube, as well as from dumps in the abandoned mines of Jugo, Iturlum and Altube, which are situated around the Murguía diapir (Fig. 1). The geological and geochemical characteristics of these deposits have been described in detail by Perona *et al.* (2018).

Tourmaline was identified in 12 of the 33 thin sections studied. The mineralogical and petrographical study was done using conventional optical microscopy and a Quanta Q-200 Scanning Electron Microscope with Energy Dispersive Spectrometry (SEM-EDS) at the Centres Científics i Tecnològics of the Universitat de Barcelona (CCiTUB). Quantitative analyses were performed by Wavelength Dispersion Spectrometry (WDS) and electron microprobe (JEOL JXA-8230) at the CCiTUB. Analytical conditions were: 20kV, a probe current of 15nA, and a 2 μ m diameter beam. The estimated accuracy and standards used were: SiO₂ (\pm 0.13%, wollastonite); Al₂O₃ (\pm 0.09%, corundum); TiO₂ (\pm 0.13%, rutile); Cr₂O₃ (\pm 0.14%, Cr₂O₃); Na₂O (\pm 0.68%, albite); MgO (\pm 0.11%, periclase); MnO (\pm 0.16%, rhodonite); FeO (\pm 0.11%, Fe₂O₃); ZnO (\pm 0.11%, sphalerite); K₂O (\pm 0.19%, feldspar); and CaO (\pm 0.02%, calcium standard). VO₃ (\pm 0.20%, vanadium metal) and F (\pm 0.50%, fluorite) were also analyzed in some samples.

Tourmaline structural formulae were calculated following Procedure 2 (appendix V in Henry et al., 2011), which consists in a normalization based on 15 cations, excluding Na, Ca, and K. It is assumed that there are no vacancies in the tetrahedral and octahedral positions (T, Z, Y) and that the amount of Li is negligible. The B₂O₃ and H₂O contents were calculated by stoichiometry assuming B=3 atoms per formula unit (a.p.f.u.) and

OH+F=4a.p.f.u. Given the chemical complexity of the mineral, a total oxide sum between 98.5% and 101.5% was considered acceptable. A total of 101 analyses were done on 60 tourmaline grains from 12 thin sections: 3 from the CTZ and 3 from the Valmaseda Fm. at Altube, 2 from the CTZ at Jugo, and 4 from the CTZ at Iturlum. Results of electron microprobe analyses are shown in Table 1.



QUATERNARY	14	
TERT.	Miocene	13
CRETACEOUS	Maastrichtian	12
		Campan.
	Lower 11	
	Coniacian	Middle 10
		Lower 9
	Turonian	Low. Upp. 8
		Upper 7
	Cenomanian	Upper 7
		Lower 6
	Albian	Upper 5
Lower 4		
TRIASSIC (Keuper)	3 1 2	

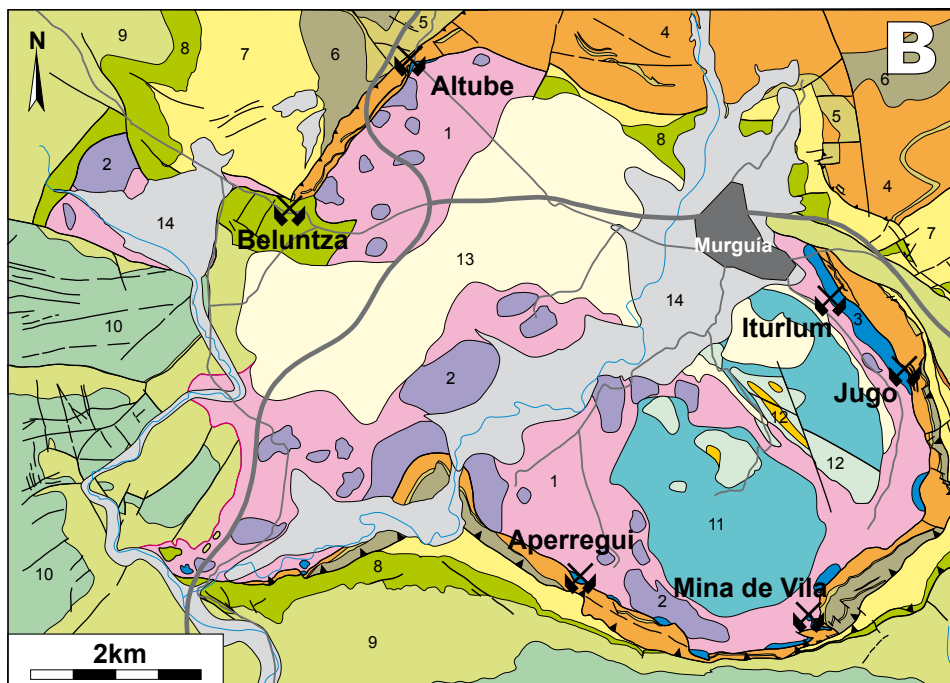


FIGURE 1. A) Geological map of the Basque Cantabrian Basin with the location of oil and gas fields, Zn-Pb and Fe deposits and the Murguía diapir. B) Geological map of the Murguía diapir with the Zn-Pb-Ba occurrences. Modified after Perona et al. (2018). 1: Evaporites and shales; 2: Ophiolites; 3: Dolomitic breccias; 4: Sandstones and shales; 5: Reefal limestones; 6: Black shales; 7, 8, 9, 10 and 11: Marls and limestones; 12: Reefal limestones; 13: Calcareous sandstones and conglomerates; 14: Sandstones and conglomerates. Valmaseda Formation: 4, 5 and 6.

TABLE 1. Microprobe analysis of tourmalines. Mean values and standard deviation

n analysis n crystals	VALMASEDA (20 Tourmalines)			ALTUBE (17 Tourmalines)			JUGO (9 Tourmalines)			ITURLUM (32 Tourmalines)			
	inherited clast	inherited nucleus	inherited edge	inherited nucleus	inherited internal halo	authigenic external halo	inherited nucleus	inherited internal halo	authigenic external halo	inherited nucleus	inherited external halo	authigenic external halo	authigenic CJT*
B ₂ O ₃ (c)	10.40(0.09)	10.35(0.11)	10.4(0.14)	10.43(0.07)	10.96(0.13)	10.88(0.09)	10.55(0.06)	11.05(0.07)	10.92(0.10)	10.61(0.08)	10.78(0.13)	10.99(0.08)	8
SiO ₂	35.98(0.54)	35.78(0.75)	36.12(0.57)	36.40(0.66)	38.98(0.49)	38.33(0.68)	37.06(0.47)	38.90(0.27)	38.30(0.65)	37.5(0.53)	37.50(0.86)	39.03(0.42)	19
Al ₂ O ₃	32.8(1.12)	31.07(2.43)	31.75(1.91)	32.07(1.39)	32.8(0.16)	33.58(1.01)	33.93(0.47)	34.03(0.21)	33.51(0.77)	32.22(1.88)	33.17(1.04)	32.77(0.39)	8
MgO	4.62(1.09)	4.57(1.69)	5.10(0.93)	5.73(1.12)	10.73(0.55)	9.71(0.48)	4.05(0.56)	10.57(0.32)	9.77(0.68)	6.15(0.74)	9.57(0.92)	11.40(0.43)	19
FeO	9.01(1.51)	10.76(1.24)	9.47(2.07)	8.01(1.07)	1.19(0.03)	1.78(0.89)	8.86(0.4)	0.67(0.46)	2.11(0.94)	7.67(1.66)	2.50(0.73)	0.21(0.29)	8
MnO	0.09(0.09)	0.09(0.07)	0.04(0.03)	0.03(0.03)	0.01(0.01)	0.00(0.01)	0.04(0.06)	0.00(0.00)	0.00(0.00)	0.03(0.02)	0.00(0.00)	0.00(0.00)	19
TiO ₂	0.68(0.28)	0.88(0.38)	0.53(0.24)	0.75(0.38)	0.00(0.00)	0.04(0.16)	0.59(0.10)	0.06(0.02)	0.10(0.26)	0.65(0.34)	0.11(0.11)	0.02(0.03)	8
Cr ₂ O ₃	0.02(0.03)	0.01(0.03)	0.01(0.03)	0.01(0.03)	0.00(0.00)	0.00(0.02)	0.04(0.05)	0.00(0.00)	0.00(0.01)	0.03(0.05)	0.03(0.03)	0.01(0.03)	19
V ₂ O ₅	n.m.	n.m.	n.m.	n.m.	n.m.	n.m.	0.06(0.05)	0.04(0.02)	0.04(0.02)	n.m.	n.m.	n.m.	8
ZnO	0.10(0.12)	0.51(0.47)	0.40(0.68)	0.03(0.03)	0.00(0.00)	0.00(0.01)	0.03(0.01)	0.03(0.00)	0.01(0.01)	0.02(0.02)	0.00(0.01)	0.00(0.01)	19
Na ₂ O	1.89(0.24)	1.94(0.16)	2.16(0.31)	1.98(0.33)	1.33(0.16)	1.43(0.35)	1.72(0.28)	1.62(0.09)	1.74(0.36)	2.12(0.28)	2.39(0.37)	2.20(0.18)	8
CaO	0.43(0.27)	0.76(0.73)	0.35(0.36)	0.50(0.30)	0.00(0.00)	0.04(0.05)	0.34(0.20)	0.12(0.03)	0.16(0.14)	0.31(0.19)	0.16(0.16)	0.10(0.32)	19
K ₂ O	0.04(0.02)	0.04(0.01)	0.02(0.01)	0.06(0.08)	0.03(0.02)	0.04(0.03)	0.02(0.01)	0.01(0.01)	0.02(0.02)	0.02(0.01)	0.04(0.05)	0.02(0.01)	8
H ₂ O (c)	3.58(0.05)	3.53(0.06)	3.58(0.05)	3.60(0.03)	3.78(0.05)	3.75(0.03)	3.58(0.09)	3.79(0.00)	3.74(0.06)	3.66(0.03)	3.72(0.04)	3.79(0.03)	19
F	n.m.	n.m.	n.m.	n.m.	n.m.	n.m.	0.05(0.07)	0.02(0.02)	0.02(0.03)	n.m.	n.m.	n.m.	8
sum Ox%	99.65(0.54)	100.32(0.62)	99.94(0.79)	99.6(0.53)	99.81(1.23)	99.6(0.77)	100.90(0.31)	100.89(0.51)	100.45(0.54)	100.98(0.52)	99.97(0.91)	100.53(0.49)	19
B(B)	3	3	3	3	3	3	3	3	3	3	3	3	8
Si(T)	6.01(0.07)	6.01(0.09)	6.03(0.08)	6.06(0.09)	6.18(0.00)	6.12(0.07)	6.10(0.05)	6.12(0.00)	6.10(0.07)	6.14(0.08)	6.04(0.10)	6.17(0.03)	19
Al(T)	0.02(0.03)	0.03(0.04)	0.02(0.04)	0.02(0.04)	0.00(0.00)	0.00(0.01)	0.00(0.00)	0.00(0.00)	0.00(0.02)	0.00(0.00)	0.02(0.05)	0.00(0.00)	8
sumAl(T)	6.03(0.05)	6.04(0.06)	6.05(0.05)	6.08(0.06)	6.18(0.00)	6.13(0.07)	6.10(0.05)	6.12(0.00)	6.10(0.05)	6.14(0.08)	6.06(0.07)	6.17(0.03)	19
Al(Z)	6.00(0.01)	5.87(0.24)	5.95(0.11)	6.00(0.01)	6.00(0)	6.00(0.01)	6.00(0.00)	6.00(0.00)	6.00(0.00)	5.94(0.11)	5.99(0.04)	6.00(0.00)	8
Mg(Z)	0.00(0.01)	0.13(0.24)	0.05(0.11)	0.00(0.01)	0.00(0.00)	0.00(0.01)	0.00(0.00)	0.00(0.00)	0.00(0.00)	0.06(0.11)	0.01(0.04)	0.00(0.00)	19
sumAl(Z)	6	6	6	6	6	6	6	6	6	6	6	6	8
Mg (Y)	1.15(0.26)	1.01(0.33)	1.22(0.26)	1.42(0.27)	2.53(0.10)	2.31(0.11)	0.99(0.14)	2.48(0.06)	2.32(0.15)	1.44(0.12)	2.29(0.18)	2.69(0.09)	19
Fe* (Y)	1.26(0.22)	1.51(0.19)	1.33(0.31)	1.12(0.15)	0.16(0.00)	0.24(0.12)	1.22(0.05)	0.09(0.06)	0.28(0.13)	1.05(0.23)	0.34(0.10)	0.03(0.04)	8
Al(Y)	0.44(0.20)	0.24(0.24)	0.28(0.22)	0.28(0.25)	0.13(0.10)	0.32(0.18)	0.59(0.06)	0.31(0.00)	0.28(0.13)	0.28(0.24)	0.30(0.15)	0.10(0.08)	19
Mn(Y)	0.01(0.01)	0.01(0.01)	0.01(0.00)	0.00(0.00)	0.00(0.00)	0.00(0.00)	0.01(0.01)	0.00(0.00)	0.00(0.00)	0.00(0.00)	0.00(0.00)	0.00(0.00)	8
Ti(Y)	0.09(0.04)	0.11(0.05)	0.07(0.03)	0.09(0.05)	0.00(0.00)	0.00(0.02)	0.07(0.01)	0.01(0.00)	0.01(0.03)	0.08(0.04)	0.01(0.01)	0.00(0.00)	19
Cr* (Y)	0.00(0.00)	0.00(0.00)	0.00(0.00)	0.00(0.00)	0.00(0.00)	0.00(0.00)	0.00(0.01)	0.00(0.00)	0.00(0.00)	0.00(0.01)	0.00(0.00)	0.00(0.00)	8
Zn(Y)	0.01(0.01)	0.06(0.06)	0.05(0.08)	0.00(0.00)	0.00(0.00)	0.00(0.00)	0.00(0.00)	0.00(0.00)	0.00(0.00)	0.00(0.01)	0.00(0.00)	0.00(0.00)	19
V(Y)	n.m.	n.m.	n.m.	n.m.	n.m.	n.m.	0.01(0.01)	0.01(0.00)	0.00(0.00)	n.m.	n.m.	n.m.	8
sumAl(Y)	2.97(0.05)	2.96(0.06)	2.95(0.05)	2.92(0.06)	2.82(0.00)	2.87(0.07)	2.90(0.05)	2.88(0.00)	2.90(0.05)	2.86(0.08)	2.94(0.07)	2.83(0.03)	19
Na(X)	0.61(0.08)	0.63(0.05)	0.70(0.11)	0.64(0.10)	0.41(0.05)	0.44(0.11)	0.55(0.09)	0.49(0.02)	0.54(0.12)	0.67(0.09)	0.75(0.12)	0.67(0.06)	8
Ca(X)	0.08(0.05)	0.14(0.13)	0.06(0.06)	0.09(0.05)	0.00(0.00)	0.01(0.01)	0.06(0.04)	0.02(0.01)	0.03(0.02)	0.05(0.03)	0.03(0.03)	0.02(0.05)	19
K(X)	0.01(0.00)	0.01(0.00)	0.00(0.00)	0.01(0.02)	0.01(0.00)	0.01(0.01)	0.00(0.00)	0.00(0.00)	0.00(0.00)	0.00(0.00)	0.01(0.01)	0.00(0.00)	8
X ₂ (X)	0.30(0.08)	0.22(0.11)	0.23(0.10)	0.26(0.11)	0.58(0.04)	0.54(0.11)	0.39(0.13)	0.49(0.02)	0.43(0.13)	0.27(0.11)	0.22(0.13)	0.30(0.08)	19
OH (V,W)	4	4	4	4	4	4	3.94(0.08)	3.98(0.03)	3.98(0.04)	4	4	4	8
F	n.m.	n.m.	n.m.	n.m.	n.m.	n.m.	0.06(0.05)	0.02(0.03)	0.02(0.04)	n.m.	n.m.	n.m.	19
Mg/(Mg+Fe)	0.48(0.10)	0.42(0.11)	0.49(0.09)	0.56(0.07)	0.94(0.00)	0.91(0.04)	0.45(0.05)	0.97(0.02)	0.89(0.05)	0.59(0.07)	0.87(0.04)	0.99(0.01)	8

"n.m.": not measured. Detection limit in wt%; FeO: 0.015; MnO: 0.015; TiO₂: 0.03; Cr₂O₃: 0.04; V₂O₅: 0.02; ZnO: 0.02; CaO: 0.08; K₂O: 0.06; F: 0.075. (*)CJT: Colorless Idiomorphic Tourmaline.

RESULTS

Petrography

Tourmaline is an accessory phase in the siliciclastic rocks of the Valmaseda Fm. and in the carbonates of the CTZ. Its crystals are colorless or green with sizes between 10 and 200 μm along the *c*-axis. Two textural types of tourmalines have been distinguished: i) sub-rounded detrital fragments with or without zoning, green and pleochroic, interpreted as inherited and ii) single idiomorphic crystals or asymmetric overgrowths (halos) on inherited grains, usually colorless (Fig. 2A), interpreted as authigenic.

Overgrowths are always in optical continuity with the inherited grain. When more than one halo is present, the first one is monopolar (Figs. 2A; 3B, C). The internal monopolar halo has a thickness of 2 to 5 μm and consists of a palisade of crystals with a length $>1\mu\text{m}$ oriented along the $+c$ -axis. Locally, a second palisade asymmetric halo, from 5 to 50 μm long in the direction of the $+c$ -axis,

is present. The crystals that make the palisade of this external halo can embrace other smaller crystals present in the rock (Fig. 2C). In the present work, when a single overgrowth has been observed, it has been considered to be an external halo.

In the calcarenites and sandstones of the Valmaseda Fm. at Altube, tourmaline appears as inherited grains, with angular to sub-rounded edges, pleochroic (green to brown colors), occasionally zoned and with solid inclusions of pyrite and quartz. Most tourmaline crystals in the CTZ from Altube and Jugo show a green pleochroic nucleus (inherited tourmaline) and colorless idiomorphic overgrowths (authigenic tourmaline). At Iturlum, most tourmalines are idiomorphic colorless crystals without a pleochroic nucleus.

Compositional data

From the primary classification based on the X-site occupancy (Henry *et al.*, 2011), differences between tourmalines from the Valmaseda Fm. and the CTZ

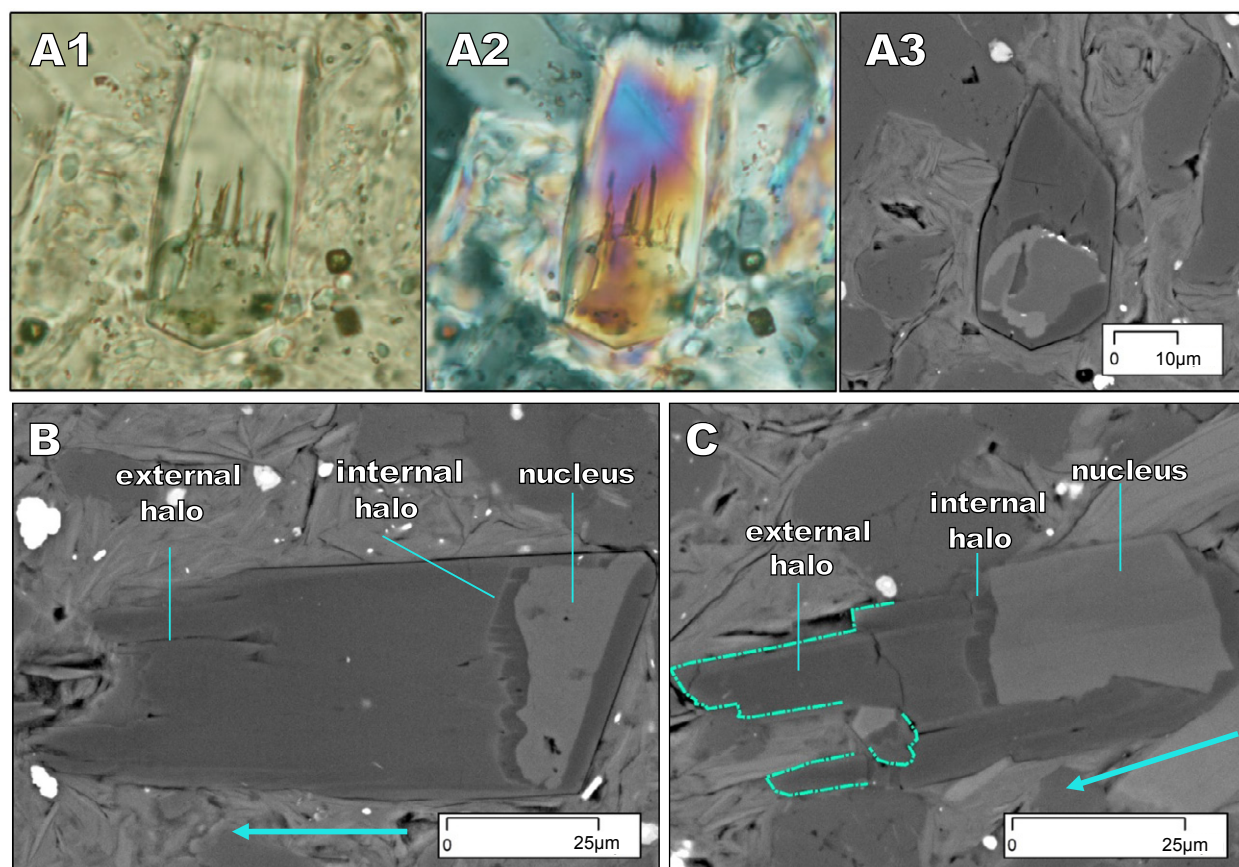


FIGURE 2. A) Tourmaline crystal with pleochroic green nucleus (inherited) and colorless (authigenic) overgrowth: A1) Photomicrograph in plane-polarized transmitted light; A2) Crossed polars; A3) Back Scattering Electron (BSE) image showing zoned nucleus and complex overgrowths (A1 and A2, same scale than in A3). B) BSE image of a tourmaline crystal with nucleus and asymmetric halos. C) BSE image of a tourmaline crystal with nucleus and asymmetric halos. Note the small tourmaline crystal encircled by the external halo. Arrow in 2B and C indicates the $+c$ axis.

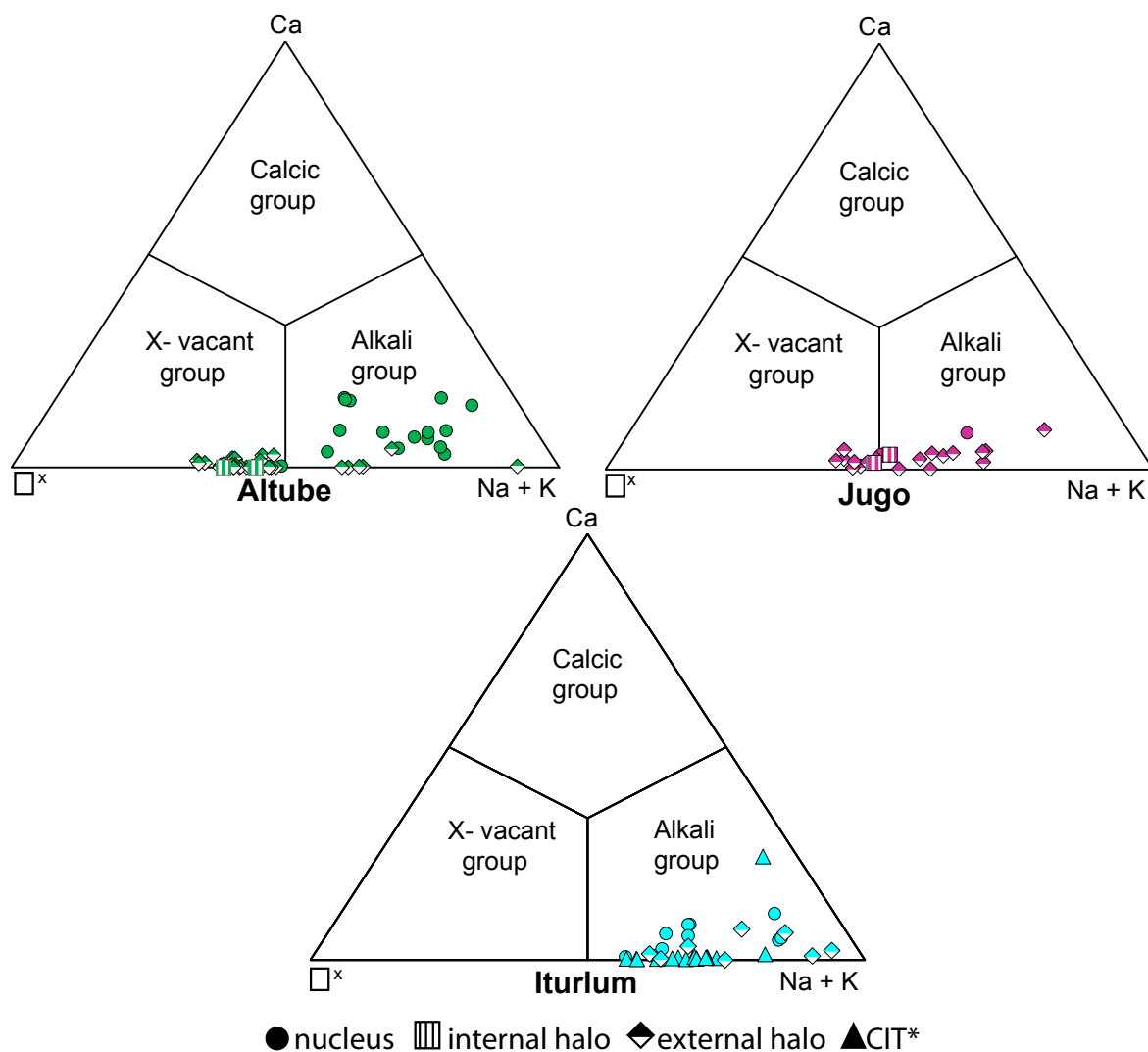


FIGURE 3. Compositional diagram of Carbonate Transition Zone (CTZ) tourmalines based on the dominance of the X position (Henry *et al.*, 2011). (*)CIT: Colorless Idiomorphic Tourmaline.

are observed. Tourmalines from the Valmaseda Fm., petrographically classified as inherited, plot within the alkaline group. In the CTZ, as the X-site occupancy of the nuclei is dominated by Na, tourmalines are also alkaline, with values of 0.64 ± 0.10 a.p.f.u. at Altube, 0.55 ± 0.09 a.p.f.u. at Jugo, and 0.67 ± 0.09 a.p.f.u. at Iturlum. In contrast, the X position in authigenic tourmalines from the CTZ, dominated by either Na or vacancy, is variable (0.54 ± 0.12 a.p.f.u., with Ca: 0.03 ± 0.02 a.p.f.u.). Tourmalines from Iturlum plot within the alkaline group, tourmalines from Jugo plot between the X-site vacancy and alkaline groups, whereas tourmaline overgrowths from Altube plot mainly within the X-site vacancy-group (Fig. 3).

According to the plot based on $Mg/(Mg+Fe)$ vs. $X\Box/(X\Box+Na)$ ratios (Henry and Dutrow, 2012),

tourmalines belong to the schorl, dravite and magnesiofoitite series. Inherited (either from Valmaseda Fm. or CTZ) and authigenic tourmalines plot on the left and right sides of the $Mg/(Mg+Fe) > 0.77$ line, respectively (Fig. 4). Tourmalines from the Valmaseda Fm. have mean $Mg/(Mg+Fe)$ ratios ranging from 0.42 ± 0.11 (core) to 0.49 ± 0.09 (edge). Nuclei of CTZ tourmalines have mean $Mg/(Mg+Fe)$ ratios of 0.56 ± 0.07 (Altube), 0.45 ± 0.05 (Jugo), and 0.59 ± 0.07 (Iturlum). Both tourmalines, Valmaseda Fm. and nuclei of CTZ, belong to the dravite and schorl series with a predominance of dravite in the nuclei of CTZ.

Compared to nuclei, authigenic tourmalines from the CTZ have a $Mg/(Mg+Fe) > 0.77$ with internal and external halos having similar $Mg/(Mg+Fe)$ ratios. Tourmaline crystals from Iturlum have $Mg/(Mg+Fe)$ ratios close to 1.

The authigenic tourmalines are Al-rich ($Al > 6a.p.f.u.$). They plot to the right of the povondraite-oxidravite join and above the schorl-dravite join, indicating that there is no substitution of Al by Fe^{3+} . In the triangular Al-Fe-Mg plot tourmalines are mostly located above the schorl-dravite line. Inherited (either from the Valmaseda Fm. or CTZ) and authigenic tourmalines plot to the left and right of the povondraite-oxidravite line, respectively (Fig. 5). All inherited tourmalines plot within the fields 2, 4, 5, and 6 of Henry and Guidotti (1985), corresponding to tourmalines associated with metapelites and granitoids; authigenic tourmalines mainly cluster within field 7.

DISCUSSION AND CONCLUSIONS

Textural and compositional differences of tourmalines from the CTZ and the Valmaseda Fm. allow us to distinguish between inherited (detrital) and authigenic origins (Figs. 2; 4). Authigenic tourmaline is present as external halos partially around detrital tourmaline or as individual crystals. The halos are asymmetrical or monopolar, typical of a low temperature environment ($\leq 300^\circ C$; Henry and Dutrow, 2012), compatible with the caprock development and the temperature of the mineralizing event (150 to $200^\circ C$) estimated by Perona *et al.* (2018) based on fluid inclusion, organic matter maturity and sphalerite-galena isotope geothermometry.

Low temperature tourmalines associated with salt domes such as for the Challenger Knoll caprock (Gulf of Mexico; Henry *et al.*, 1999), or for the Alto Chaparé caprock in Cochabamba (Bolivia; Žáček *et al.*, 2000) are Al-deficient due to the replacement of Al by Fe^{3+} . In the Al-Fe-Mg diagram they plot upon the povondraite-oxidravite join and below the schorl-dravite join (Fig. 5). They are also Na and O rich in the X and W positions, respectively, as expected for tourmalines formed under hypersaline and oxidizing conditions associated with evaporites. These chemical features are also shared by tourmalines in meta-evaporites at Liaoning (China) and Stolzenfeld (Namibia; Henry *et al.*, 2008) and by tourmalines formed in oxidizing hypersaline environments associated with boiling processes such as in porphyry Cu deposits (Baksheev *et al.*, 2011; Henry and Dutrow, 2012).

Differently, the studied authigenic tourmalines from the Murguía diapir are Al-rich and plot to the right of the povondraite-oxidravite join and above the schorl-dravite join. This indicates that there is no substitution of Al by Fe^{3+} which occurs when the Fe^{3+}/Fe^{2+} ratio in the fluid is low, typical of reducing conditions (Baksheev *et al.*, 2011; Hazarika *et al.*, 2015; Ranta *et al.*, 2017). According to Henry *et al.* (2008), when sulfur is available precipitation of iron sulfide may occur,

decreasing the iron content in the fluid, and consequently in the tourmaline. At Murguía, this condition could prevail during the sulfate reduction process associated with the formation of the caprock, or even later, related to the hydrothermal event that resulted in the sulfide mineralization.

Inherited tourmalines from the studied localities plot within the alkaline (Na+K) group field. In contrast, authigenic tourmalines show different X-site occupancy (Fig. 3): tourmalines from Iturlum plot within the alkaline group, tourmaline overgrowths from Altube plot within the X-site vacancy, and tourmalines from Jugo overlap both fields. Indeed, according to Perona *et al.* (2018), at Iturlum, mineralization is constituted by barite, an early phase in the paragenetic sequence, partially replaced by dolomite. At Altube, pyrite, sphalerite, galena, and saddle dolomite are the main mineral phases, whereas barite is scarce. The Jugo deposit shares mineralogical characteristics with the Iturlum and Altube deposits, including barite, sulfides, albite, and several dolomite generations. Therefore, the apparent relationship between mineralogy and tourmaline chemistry suggests that the variation of the Na content in the X position for the authigenic tourmalines around the Murguía diapir records the chemical changes in the fluid, as previously shown by Henry and Dutrow (2012) for low-temperature environments.

Compared to inherited ones, authigenic tourmalines are richer in Mg ($Mg/(Mg+Fe) > 0.7$), with the highest

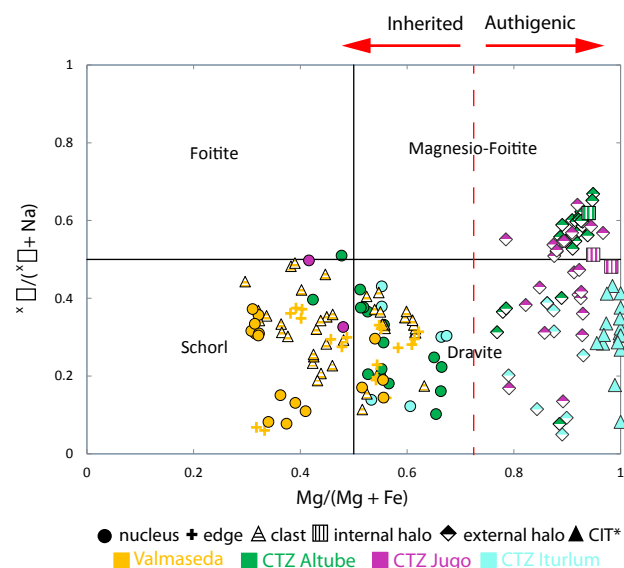


FIGURE 4. Classification diagram for tourmalines with a small amount of Ca and F in positions X and W, respectively (Henry and Dutrow, 2012). Dashed line separates authigenic and inherited tourmalines. (*)CIT: Colorless Idiomorphic Tourmaline; CTZ: Carbonate Transition Zone.

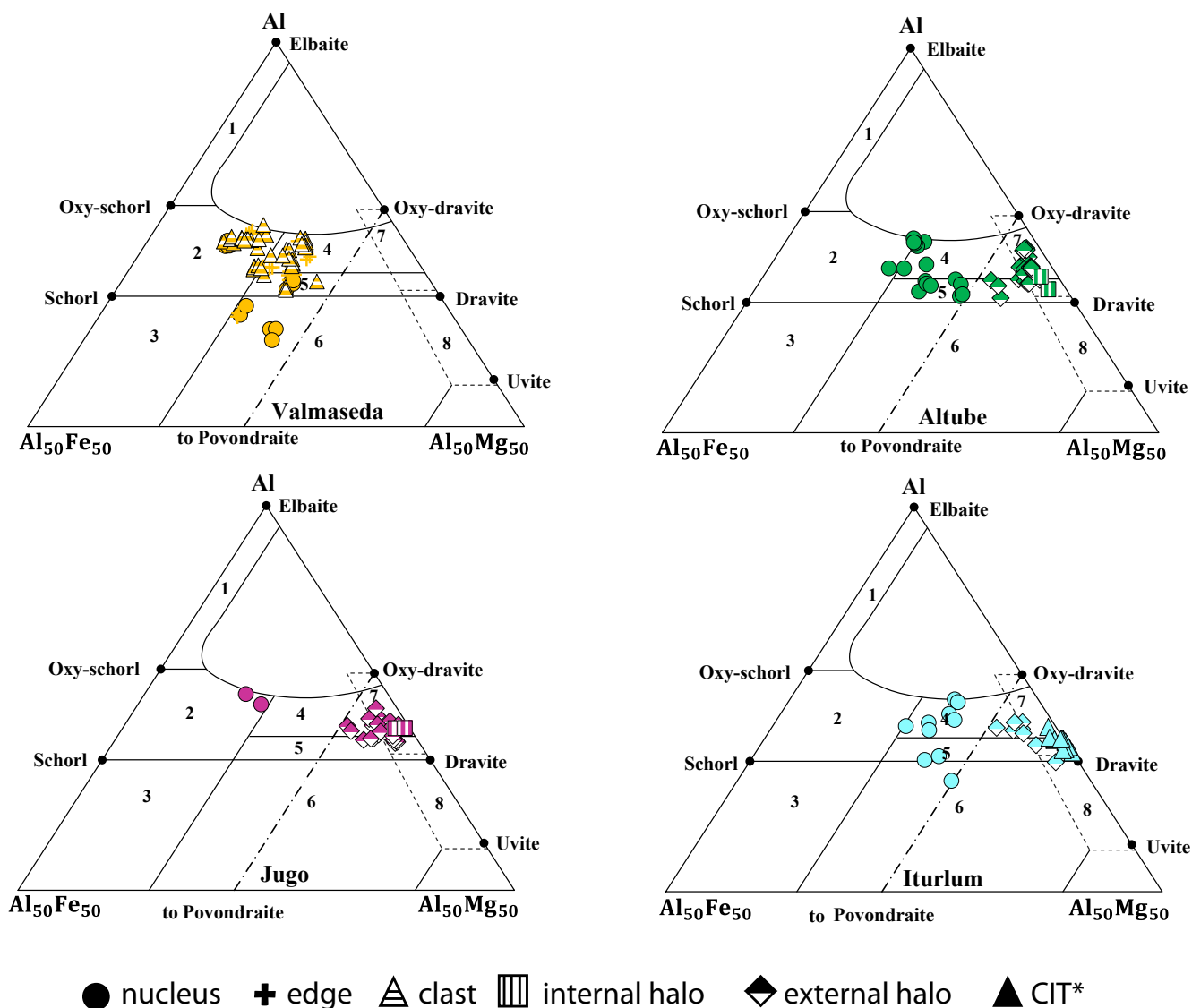


FIGURE 5. Compositional variation of tourmalines from the Valmaseda and Carbonate Transition Zone at Altube, Jugo and Iturlum, in the [Henry and Guidotti \(1985\)](#) Al-Fe(tot)-Mg plot. 1) Li-rich granitoid pegmatites and aplites; 2) Li-poor granitoids and their associated pegmatites and aplites; 3) Fe³⁺-rich quartz-tourmaline rocks (hydrothermally altered granites); 4) Metapelites and metapsammities coexisting with an Al-saturating phase; 5) Metapelites and metapsammities not coexisting with an Al-saturating phase; 6) Fe³⁺-rich quartz-tourmaline rocks, calc-silicate rocks, and metapelites; 7) Low-Ca metaultramafics and Cr-, V-rich metasediments; and 8) Metacarbons and meta-pyroxenites. (*)CIT: Colorless Idiomorphic Tourmaline.

values obtained at Iturlum (Table 1). Considering that at Iturlum dolomite is a minor phase and sulfides (pyrite) are almost absent, and that Zn-Pb mineralization around the Murguía diapir is related to dolomitization, it is conceivable that differences in the Mg/Mg+Fe ratios of tourmalines might reflect the dolomitization progress.

From the presented data, we can conclude that textures and chemical compositions of authigenic tourmalines from the CTZ and Valmaseda Fm. around the Murguía diapir may be used as tracers of hydrothermal fluid circulation. Their chemical compositions indicate mineral growth under

reducing conditions, compatible with the hydrothermal event responsible for Zn-Pb sulfide deposition and caprock formation during the diapir ascent.

ACKNOWLEDGMENTS

The authors would like to thank two anonymous referees for their constructive comments which helped to improve the manuscript. The present work is a contribution of the “Mineralogía Aplicada i Geoquímica de Fluids” 2017SGR-1733 Research Group.

REFERENCES

- Baksheev, I.A., Prokof'ev, V.Y., Yapaskurt, V.O., Vigasina, M.F., Zorina, L.D., Solov'ev, V.N., 2011. Ferric-iron-rich tourmaline from the Darasun gold deposit, Transbaikalia, Russia. *The Canadian Mineralogist*, 49(1), 263-276.
- Dutrow, B.L., Henry, D.J., 2011. Tourmaline: A geological DVD. *Elements*, 7(5), 301-306.
- Griffin, W.L., Slack, J.F., Ramsden, A.R., Win, T.T., Ryan, C.G., 1996. Trace elements in tourmalines from massive sulfides deposits and tourmalinites; geochemical controls and exploration applications. *Economic Geology*, 91(4), 657-675.
- Hazarika, P., Mishra, B., Pruseth, K.L., 2015. Diverse tourmaline compositions from orogenic gold deposits in the Hutti-Maski Greenstone Belt, India: implications for sources of ore-forming fluids. *Economic Geology*, 110(2), 337-353.
- Henry, D.J., Guidotti, C.V., 1985. Tourmaline as a petrogenetic indicator mineral- An example from the staurolite-grade metapelites of NW Maine. *American Mineralogist*, 70(1-2), 1-15.
- Henry, D.J., Kirkland, B.L., Kirkland, D.W., 1999. Sector-zoned tourmaline from the cap rock of a salt dome. *European Journal of Mineralogy*, 11(2), 263-280.
- Henry, D.J., Sun, H., Slack, J.F., Dutrow, B.L., 2008. Tourmaline in meta-evaporites and highly magnesian rocks: perspectives from Namibian tourmalinites. *European Journal of Mineralogy*, 20(5), 889-904.
- Henry, D.J., Novák, M., Hawthorne, F.C., Ertl, A., Dutrow, B.L., Uher, P., Pezzotta, F., 2011. Nomenclature of the tourmaline-supergrupp minerals. *American Mineralogist*, 96(5-6), 895-913.
- Henry, D.J., Dutrow, B.L., 2012. Tourmaline at diagenetic to low-grade metamorphic conditions: Its petrologic applicability. *Lithos*, 154, 16-32.
- Perona, J., Canals, À., Cardellach, E., 2018. Zn-Pb Mineralizations associated with salt diapirs in the Basque-Cantabrian Basin (N Spain): Geology, geochemistry and genetic model. *Economic Geology*, 113(5), 1133-1159.
- Ranta, J., Hanski, E., Cook, N., Lahaye, Y., 2017. Source of boron in the Palokas gold deposit, northern Finland: evidence from boron isotopes and major element composition of tourmaline. *Mineralium Deposita*, 52(5), 733-746.
- Slack, J.F., Trumbull, R.B., 2011. Tourmaline as a recorder of ore-forming processes. *Elements*, 7(5), 321-326.
- Tavani, S., Muñoz, J.A., 2012. Mesozoic rifting in the Basque-Cantabrian Basin (Spain): Inherited faults, transversal structures and stress perturbation. *Terra Nova*, 24(1), 70-76.
- van Hinsberg, V.J., Henry, D.J., Marschall, H.R., 2011. Tourmaline: an ideal indicator of its host environment. *The Canadian Mineralogist*, 49(1), 1-16.
- von Goerne, G., Franz, G., Heinrich, W., 2001. Synthesis of tourmaline solid solutions in the system Na₂O-MgO-Al₂O₃-SiO₂-B₂O₃-H₂O-HCl and the distribution of Na between tourmaline and fluid at 300 to 700°C and 200 MPa. *Contributions to Mineralogy and Petrology*, 141(2), 160-173. DOI: 10.1007/s004100100243
- Žáček, V., Frýda, J., Petrov, A., Hyršl, J., 2000. Tourmalines of the povondraite- (oxy)dravite series from the cap rock of meta-evaporite in Alto Chapare, Cochabamba, Bolivia. *Journal of Czech Geological Society*, 45(1-2), 3-12.

Manuscript received October 2018;

revision accepted May 2019;

published Online June 2019.